

# Nanoscale

Accepted Manuscript



This is an *Accepted Manuscript*, which has been through the Royal Society of Chemistry peer review process and has been accepted for publication.

*Accepted Manuscripts* are published online shortly after acceptance, before technical editing, formatting and proof reading. Using this free service, authors can make their results available to the community, in citable form, before we publish the edited article. We will replace this *Accepted Manuscript* with the edited and formatted *Advance Article* as soon as it is available.

You can find more information about *Accepted Manuscripts* in the [Information for Authors](#).

Please note that technical editing may introduce minor changes to the text and/or graphics, which may alter content. The journal's standard [Terms & Conditions](#) and the [Ethical guidelines](#) still apply. In no event shall the Royal Society of Chemistry be held responsible for any errors or omissions in this *Accepted Manuscript* or any consequences arising from the use of any information it contains.

Electronic Supplementary Information

**Nucleation-Mediated Synthesis and Enhanced Catalytic  
Properties of Au-Pd Bimetallic Tripods and Bipyramids with  
Twinned Structures and High-Energy Facets**

Lei Zhang,<sup>\*a</sup> Xue Wang,<sup>b</sup> Qiaoli Chen<sup>b</sup> and Zhiyuan Jiang<sup>\*b</sup>

*<sup>a</sup>Key Laboratory for Green Chemical Technology of Ministry of Education, School of  
Chemical Engineering and Technology, Tianjin University, Collaborative Innovation Center  
of Chemical Science and Engineering, Tianjin 300072, China*

*E-mail: zhangl@tju.edu.cn*

*<sup>b</sup>State Key Laboratory for Physical Chemistry of Solid Surfaces & Department of Chemistry,  
College of Chemistry and Chemical Engineering, Xiamen University, Xiamen 361005, China*

*E-mail: zyjiang@xmu.edu.cn*

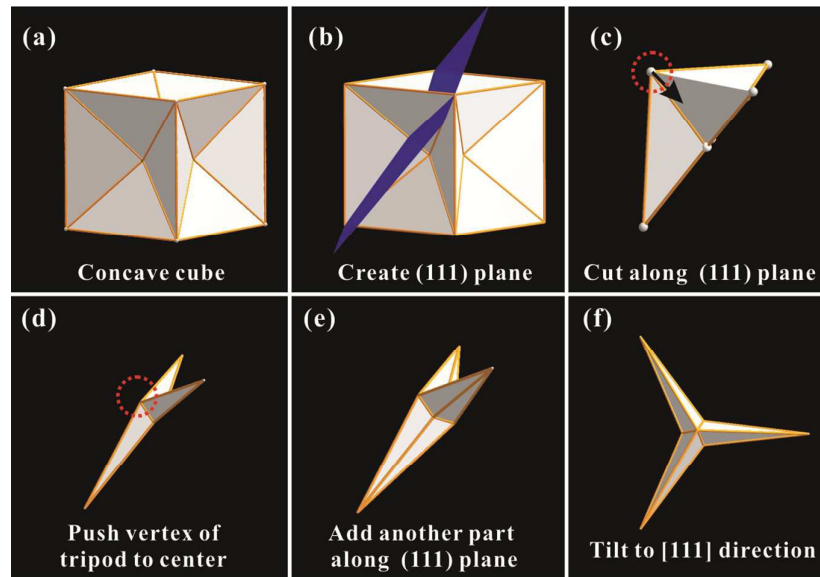


**Fig. S1** The models showing that the tripods exposed by  $\{hkk\}$  facets are evolved from a concave cubic structure.

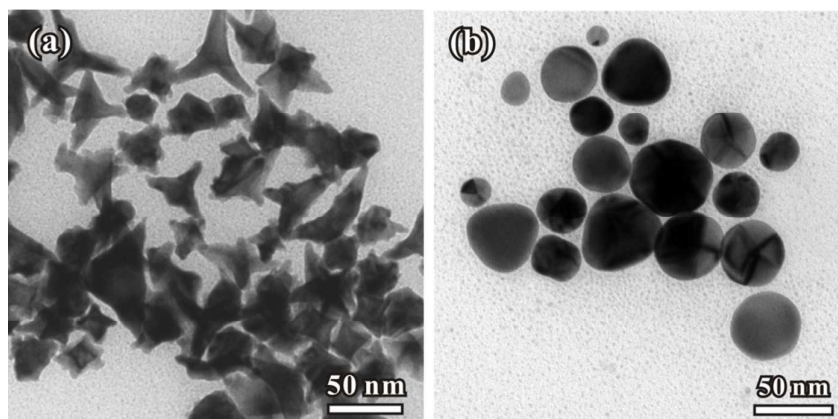


**Fig. S2** (a) TEM image of Au-Pd NCs that were prepared using the standard procedure, expect for the introduced  $\text{H}_2\text{PdCl}_4$  increased to 1 mL. (b) TEM image of Au NCs that were prepared using the standard procedure, expect for the absence of  $\text{H}_2\text{PdCl}_4$ .

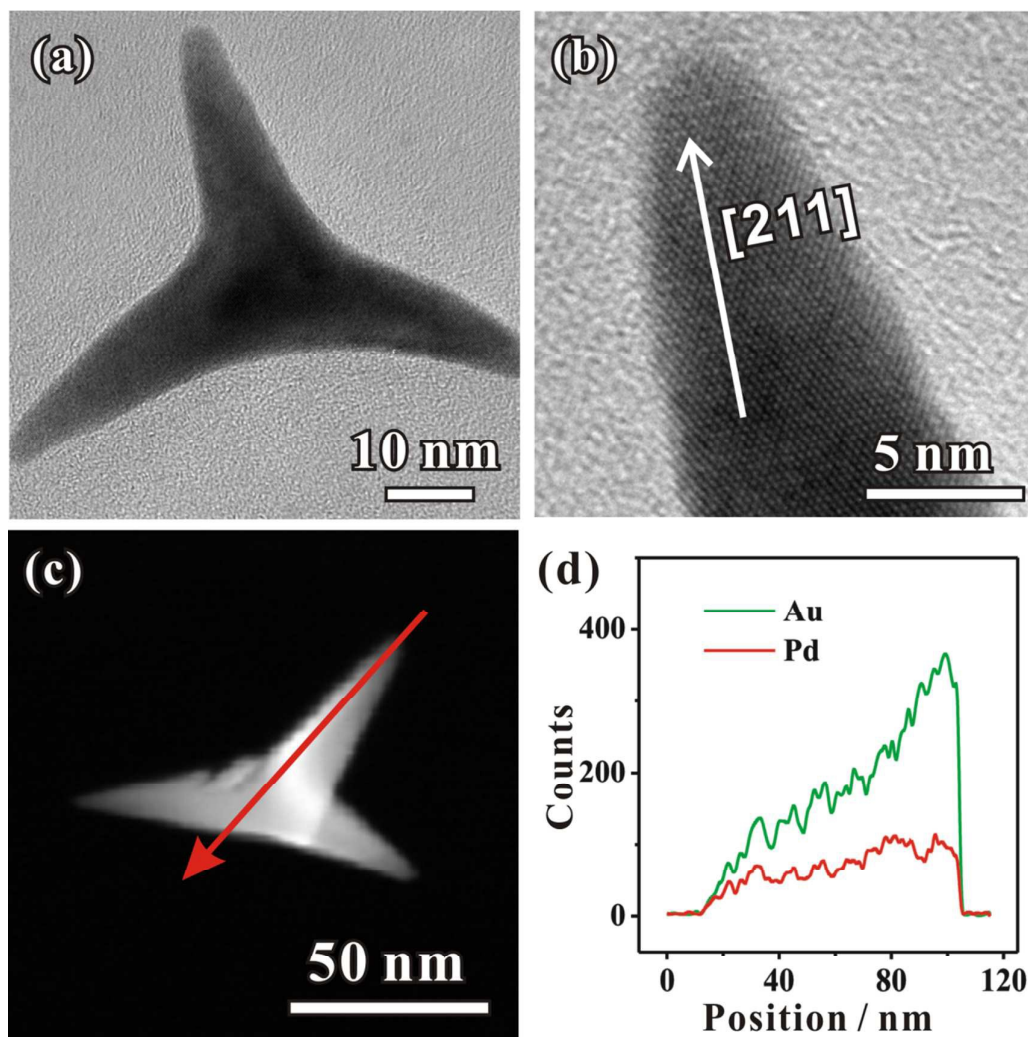


**Fig. S3** (a, b) The HR-TEM images of one individual tripod viewing along  $\langle 111 \rangle$  direction. (c, d) The cross-sectional compositional line-scanning profile of the Au-Pd tripods.

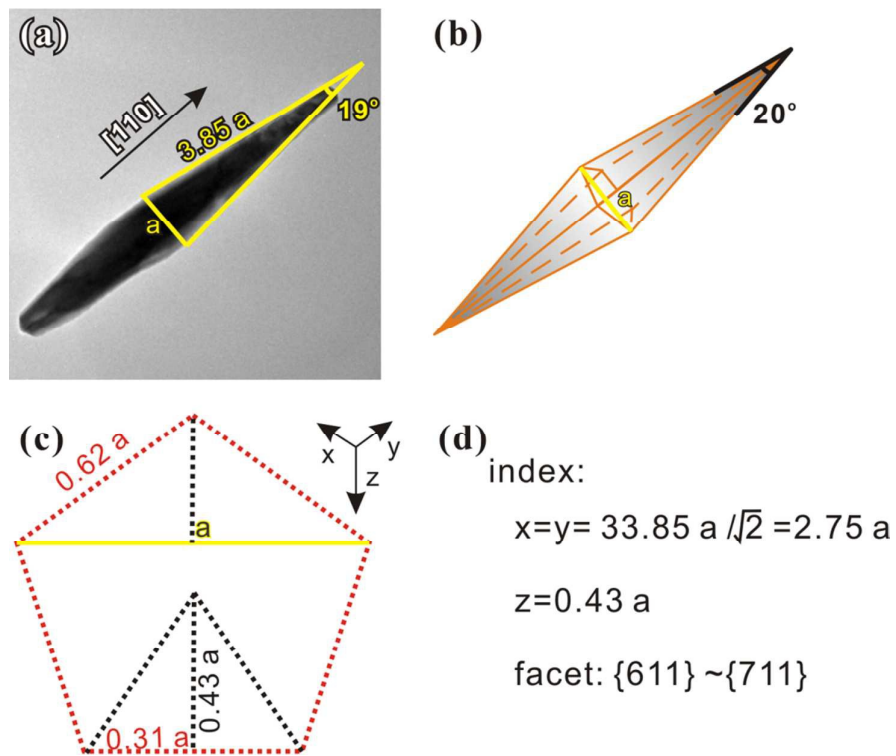


**Fig. S4** (a, b) The TEM image of one individual bipyramid and corresponding schematic model. (c, d) The calculation of the geometric parameters of bipyramid conclude that the surfaces of bipyramids range from  $\{611\}$  to  $\{711\}$  facets.

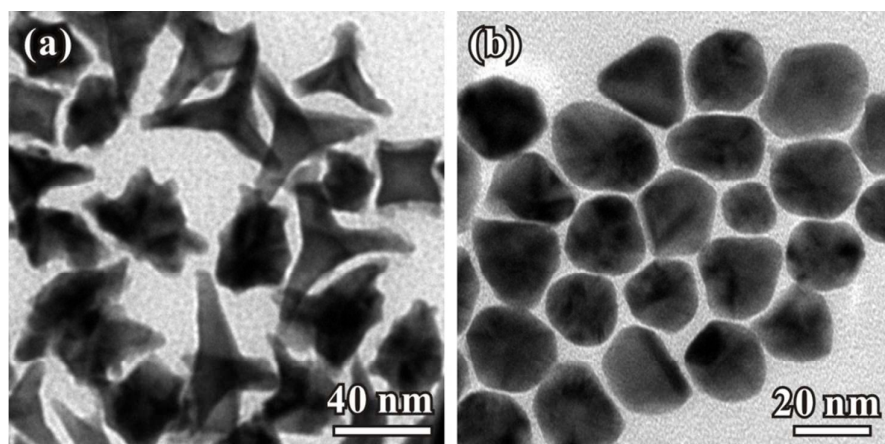
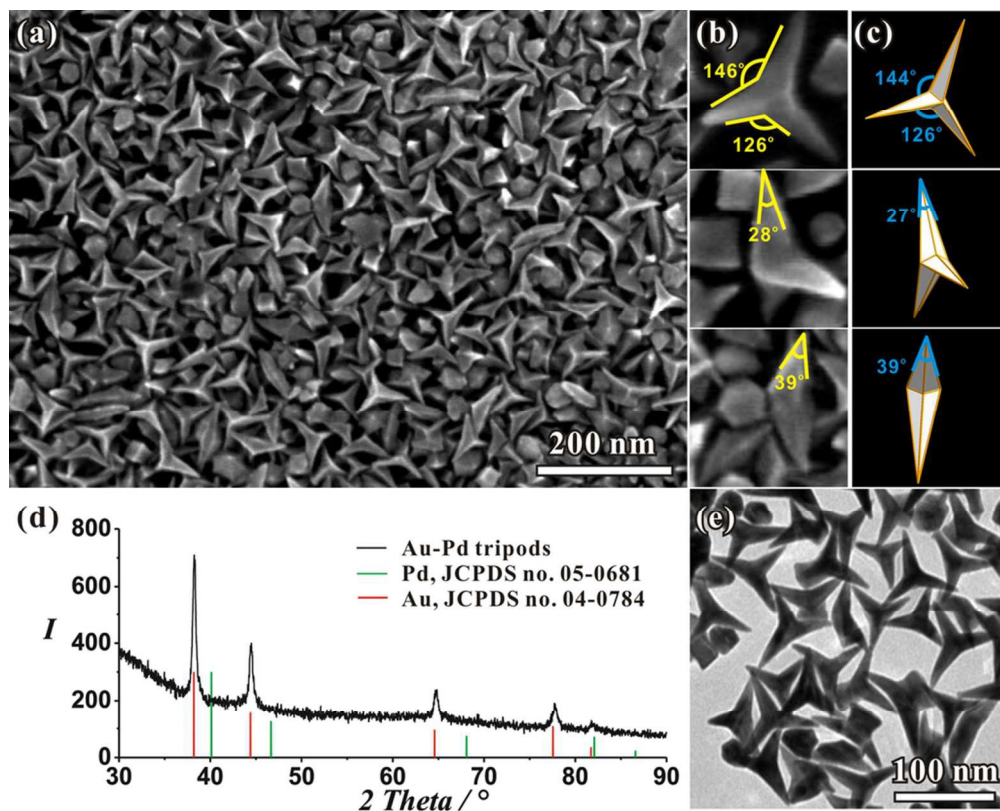
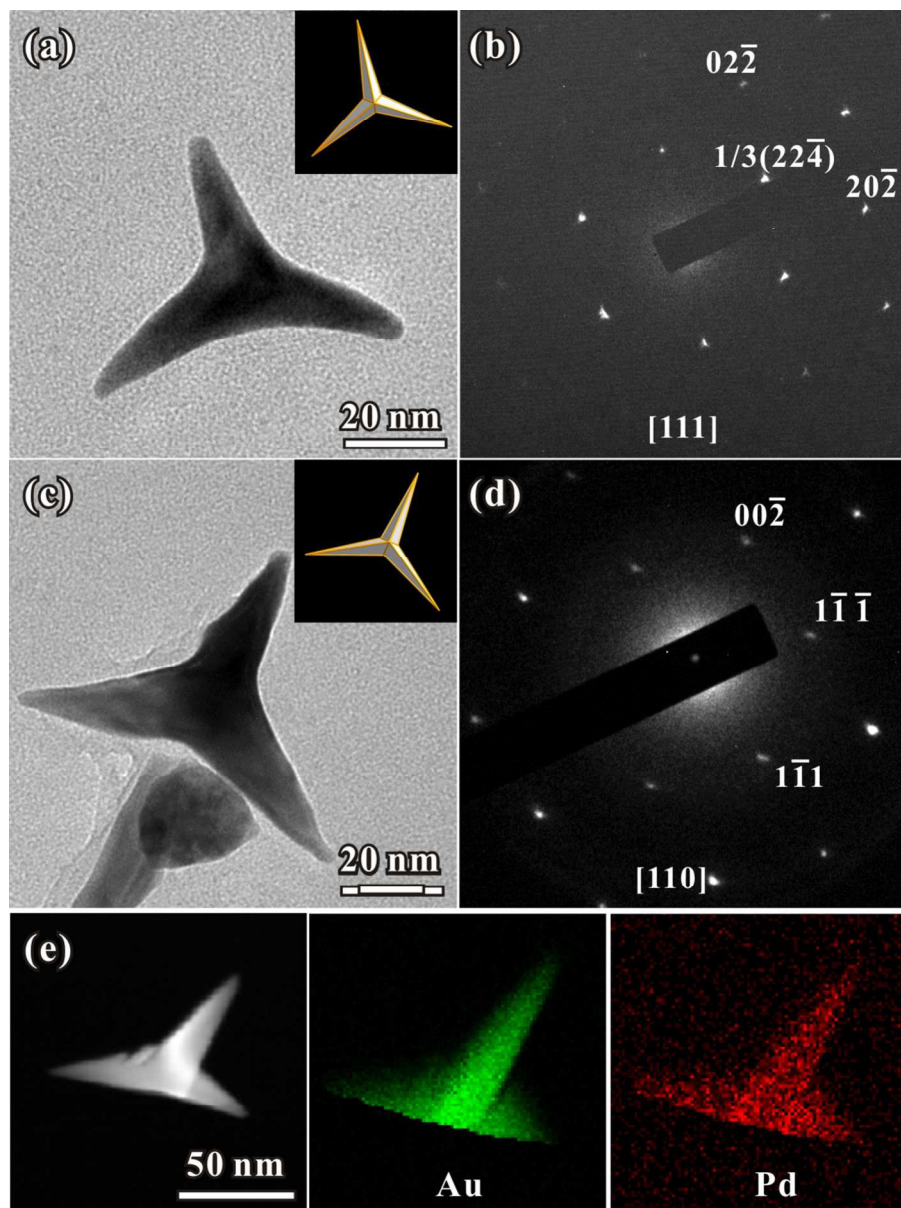


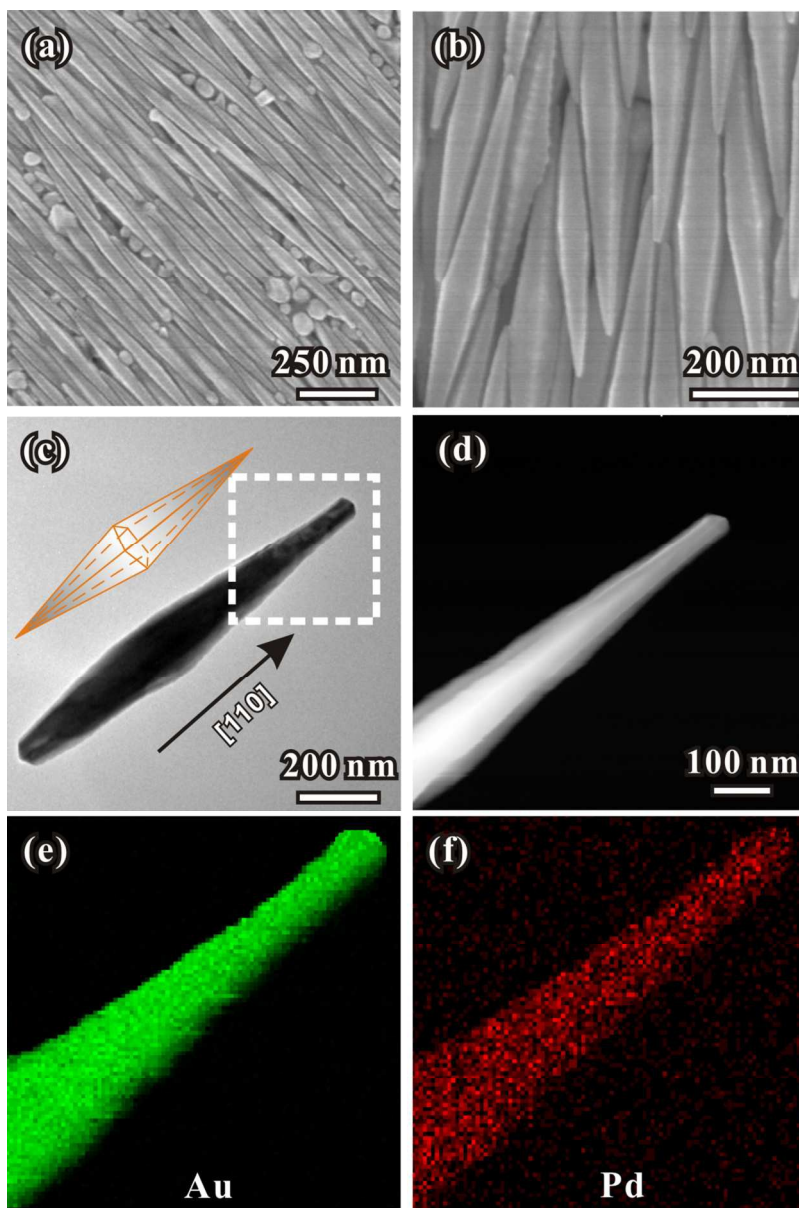
**Fig. S5** (a) TEM image of Au-Pd bimetallic nanocrystals that were prepared using the standard procedure, expect in the absence of  $\text{Cu}(\text{CH}_3\text{COO})_2$ . (b) TEM image of spherical Au-Pd nanocrystals that were prepared using the standard procedure, expect adding 2 mL of  $\text{Cu}(\text{CH}_3\text{COO})_2$  into the solution.



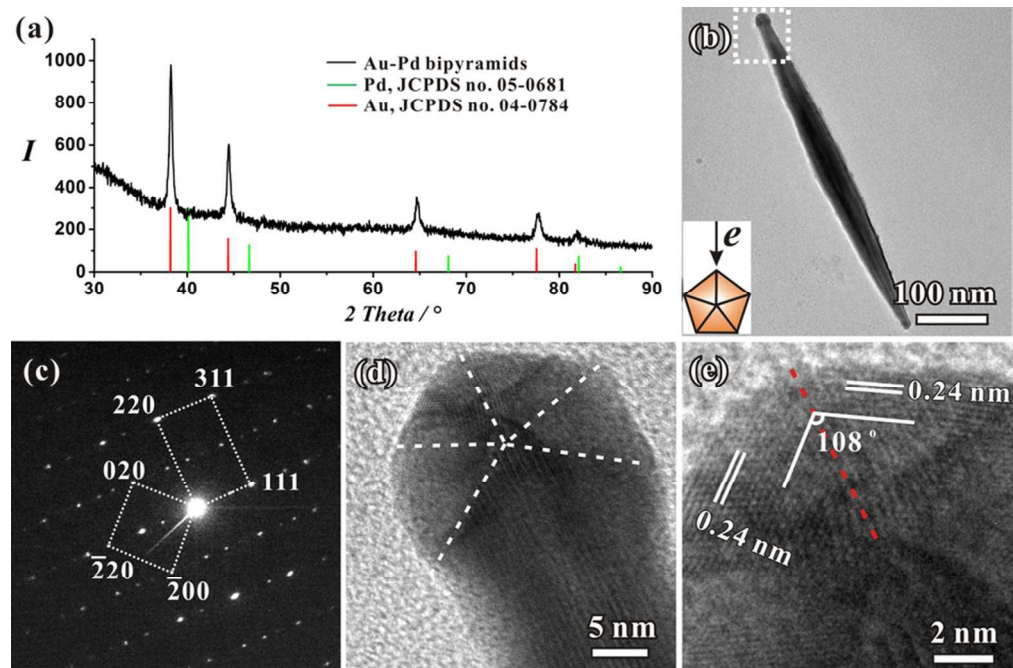
87x69mm (300 x 300 DPI)



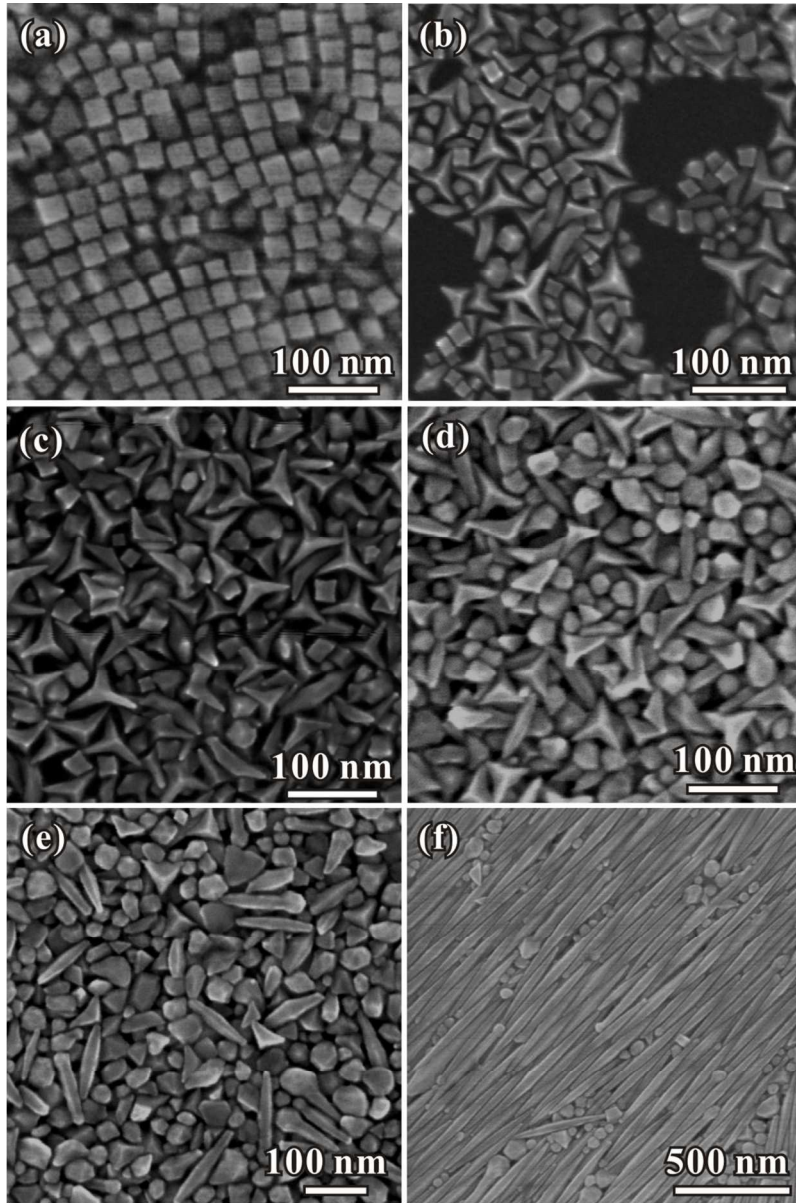
106x142mm (300 x 300 DPI)



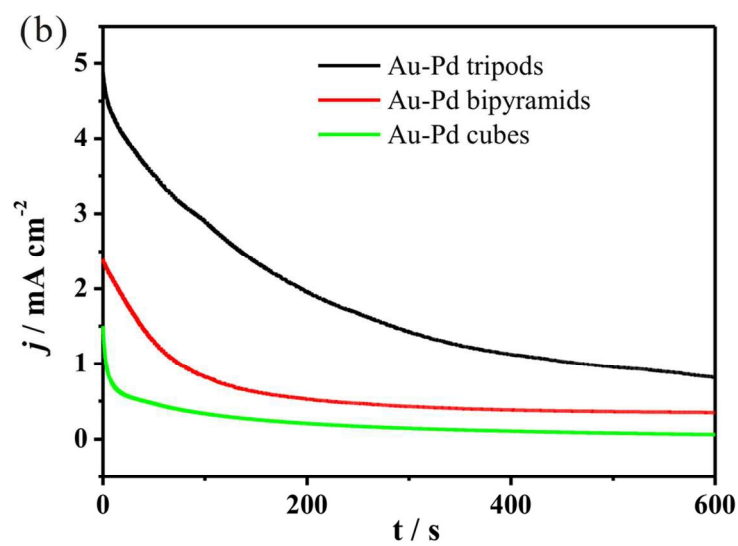
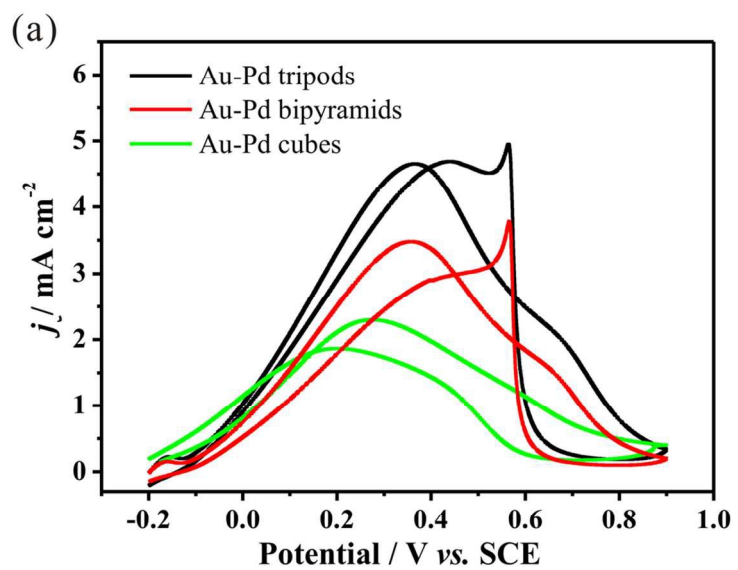
119x180mm (300 x 300 DPI)



79x53mm (300 x 300 DPI)



113x171mm (300 x 300 DPI)



106x142mm (300 x 300 DPI)



Journal Name

ARTICLE

## Nucleation-Mediated Synthesis and Enhanced Catalytic Properties of Au-Pd Bimetallic Tripods and Bipyramids with Twinned Structures and High-Energy Facets

Received 00th January 20xx,  
Accepted 00th January 20xx

DOI: 10.1039/x0xx00000x

www.rsc.org/

Lei Zhang,<sup>\*a</sup> Qiaoli Chen,<sup>b</sup> Xue Wang<sup>b</sup> and Zhiyuan Jiang<sup>\*b</sup>

Au-Pd alloy has been proved to be an excellent catalyst in many applications, such as the electro-oxidation of formic acid, CO oxidation and oxidation of alcohols to aldehydes. However, most of the researches were focused on the shape-controlled Au-Pd alloy NCs with single-crystal structure. Due to the existence of high-energy atoms on the twin defects, twinned structures usually will further increase their catalytic activities. It is necessary to develop a method to prepare Au-Pd alloy with twinned structures and investigate their catalytic properties. Herein, we successfully synthesized Au-Pd alloy tripods and bipyramids with twinned structures by the cooperation of cetyltrimethyl trimethyl ammonium chloride (CTAC) and cetyltrimethyl trimethyl ammonium bromide (CTAB). The tripods contain one twin plane, while the bipyramids are consisted of fivefold-twinned structure. In addition, the tripods and bipyramids are both exposed by high-energy facets. We proposed that the tripods and bipyramids are evolved from bipyramid seeds and fivefold twinned seeds, respectively. The as-prepared Au-Pd tripods and bipyramids performed better activity for electrocatalytic oxidation of formic acid compared to the cubic Au-Pd nanoparticles.

### Introduction

Noble metal nanocrystals (NCs) have been applied in many important industrial areas due to their physical and chemical properties.<sup>1-9</sup> Recently, multi-component noble metal nanostructures have attracted an increasing number of attention, as their properties (such as catalysis) could be enhanced by the synergistic effects between different components.<sup>10-16</sup> For example, Au-Pd bimetallic NCs were proved to be an excellent catalyst in many applications, such as the electro-oxidation of formic acid, CO oxidation and oxidation of alcohols to aldehydes.<sup>17-22</sup>

The controlled synthesis of Au-Pd alloy NCs with well-defined morphologies is of great importance to optimize the properties of Au-Pd catalysts. According to crystal growth theory, the most stable Au-Pd structures are exposed by {111} or {100} low-energy facets.<sup>23,24</sup> With the in-depth

understanding of reaction mechanism, the synthesis of NCs with high-energy facets were greatly developed. It has been widely reported that structures enclosed by high-energy facets usually exhibit excellent performance in many catalytic reactions due to their high density of atomic steps, ledges and kinks on the surface.<sup>25-34</sup> There have also been a few successes in the preparation of Au-Pd bimetallic NCs with high-energy facets, such as {hhl} and {hkl} facets. For example, we successfully synthesized hexoctahedral (HOH) Au-Pd alloy exposed by {hkl} facets with the assistance of Cu<sup>2+</sup>.<sup>17</sup> Han and co-workers can also obtain HOH Au-Pd alloy NCs through co-reduction of Au and Pd precursors using ascorbic acid in the presence of cetyltrimethyl ammonium chloride.<sup>18</sup> Inspired by this, our group has demonstrated a route to prepare monodisperse Au-Pd alloy NCs with systematic shape evolution from rhombic dodecahedral to trisoctahedral (TOH), and HOH structures by varying the concentration of octadecyltrimethyl ammonium chloride in a surfactant-mediated synthesis.<sup>22</sup>

It should be pointed that, almost all of the studies about Au-Pd alloy NCs focused on single-crystal structures. Single-twinned or multiply-twinned structures contain high-energy atoms on the twin defects and will greatly increase their catalytic activities.<sup>35-37</sup> Unfortunately, due to the complex process during nucleation, Au-Pd alloy NCs with twinned planes are rarely reported. Therefore, it is essential to develop a method to prepare Au-Pd alloy with twinned structures and investigate their catalytic properties. To approach a NC with twinned structure, the nucleation process should be precise controlled to favour the fabrication of single-twinned or

<sup>a</sup>Key Laboratory for Green Chemical Technology of Ministry of Education, School of Chemical Engineering and Technology, Tianjin University, Collaborative Innovation Center of Chemical Science and Engineering, Tianjin 300072, China

<sup>b</sup>State Key Laboratory of Physical Chemistry of Solid Surfaces, Collaborative Innovation Center of Chemistry for Energy Materials, and Department of Chemistry, College of Chemistry and Chemical Engineering, Xiamen University, Xiamen 361005, China

zhangl@tju.edu.cn; zyjjiang@xmu.edu.cn

Electronic Supplementary Information (ESI) available: [The models showing that the tripods are evolved from a concave cubic structure; the cross-sectional compositional line-scanning profile of the Au-Pd tripods; TEM images of Au-Pd alloy obtained with different amount of Cu(CH<sub>3</sub>COO)<sub>2</sub> introduced. This material is available free of charge via the Internet at <http://pubs.acs.org>]. See DOI: 10.1039/b000000x/

multiply-twinned seeds. In this paper, we successfully stabilized single-crystal, single twinned, or multiply twinned structure with the cooperation of cetyltrimethyl trimethyl ammonium chloride (CTAC) and cetyltrimethyl trimethyl ammonium bromide (CTAB). After overgrowth process, the seeds with multiple structures evolved to nanocubes, tripods and bipyramids respectively. In addition, the tripods and bipyramids are exposed by {411} and {611}~{711} high-energy facets. According to our best knowledge, the Au-Pd alloy NCs exposed by high-energy surfaces, together with twinned structures have not been reported yet. Furthermore, the as-prepared Au-Pd tripods and bipyramids both exhibited excellent performance towards electrocatalytic oxidation of formic acid.

## Experimental section

### Materials

Chloroauric acid hydrated ( $\text{HAuCl}_4 \cdot 4\text{H}_2\text{O}$ , analytical grade), L-ascorbic acid (AA, analytical grade), Cetyltrimethyl trimethyl ammonium chloride (CTAC, 99%), Cetyltrimethyl trimethyl ammonium bromide (CTAB, 99%), copper(II) acetate ( $\text{Cu}(\text{CH}_3\text{COO})_2$ , analytical grade) and hydrochloric acid (HCl, analytical grade) were purchased from Sinopharm Chemical Reagent Co. Ltd. (Shanghai, China). Palladium(II) chloride ( $\text{PdCl}_2$ , analytical grade) was purchased from Shanghai fine chemical materials institute. All reagents were used as received without further purification. All aqueous solutions were prepared with ultrapure water.

### Preparation of 1 mM $\text{H}_2\text{PdCl}_4$ solution

The  $\text{H}_2\text{PdCl}_4$  solution ( $10 \text{ mmol L}^{-1}$ ) was prepared by dissolving  $\text{PdCl}_2$  (0.1773 g) in a HCl ( $0.2 \text{ mol L}^{-1}$ , 10 mL) solution and further diluting it to 100 mL with ultrapure water. A  $\text{H}_2\text{PdCl}_4$  solution ( $1 \text{ mmol L}^{-1}$ ) was prepared by diluting a  $\text{H}_2\text{PdCl}_4$  solution ( $10 \text{ mmol L}^{-1}$ ) with ultrapure water.

### Synthesis of Au-Pd Bimetallic Tripods and Bipyramids

In a standard procedure for the synthesis of Au-Pd tripods, an aqueous  $\text{H}_2\text{PdCl}_4$  solution ( $0.3 \text{ mL}$ ,  $1.0 \text{ mmol L}^{-1}$ ), a CTAC aqueous solution ( $2.7 \text{ mL}$ ,  $0.04 \text{ mol L}^{-1}$ ) and a CTAB aqueous solution ( $0.3 \text{ mL}$ ,  $0.04 \text{ mol L}^{-1}$ ) was added into an aqueous  $\text{HAuCl}_4$  solution ( $3.0 \text{ mL}$ ,  $1.0 \text{ mmol L}^{-1}$ ) in turn. Then, an aqueous  $\text{Cu}(\text{CH}_3\text{COO})_2$  solution ( $1.0 \text{ mmol L}^{-1}$ ) of  $0.30 \text{ mL}$  was added into the solution. After homogeneous mixing, a freshly prepared, aqueous AA solution ( $0.20 \text{ mL}$ ,  $0.10 \text{ mol L}^{-1}$ ) was quickly added with a gentle shaking to this solution and left undisturbed for 3 hours at  $23 \text{ }^\circ\text{C}$ . After the reaction, the samples were centrifuged at  $6000 \text{ rpm}$  for 10 min and washed by ultrapure water for two times.

For the preparation of Au-Pd bipyramids, the introduced CTAC aqueous solution ( $2.7 \text{ mL}$ ,  $0.04 \text{ mol L}^{-1}$ ) and CTAB aqueous solution ( $0.3 \text{ mL}$ ,  $0.04 \text{ mol L}^{-1}$ ) were changed to the introduction of only a CTAB aqueous solution ( $3.0 \text{ mL}$ ,  $0.04 \text{ mol L}^{-1}$ ).

### Structural characterizations.

The morphology and structure of the products were characterized by scanning electron microscopy (SEM, Hitachi S-4800), transmission electron microscopy (TEM, JEOL JEM-2100) and X-ray powder diffraction (XRD, Panalytical X-pert diffractometer with  $\text{Cu-K}\alpha$  radiation). The high angle annular dark field scanning transmission electron microscopy energy dispersive X-ray spectroscopy (HAADF-STEM-EDS) was performed on a FEI TECNAI F30 microscope operated at  $300 \text{ kV}$ .

### Electrochemical measurement.

A glassy carbon electrode (diameter of  $3 \text{ mm}$ ) was carefully polished and washed before every experiment.  $5 \mu\text{L}$  of the ethanol suspensions of the as-prepared Au-Pd alloy NCs ( $0.20 \text{ mg/mL}$ ) were dripped onto the surface of the glassy carbon electrode and dried in an oven at  $50 \text{ }^\circ\text{C}$ . Cyclic voltammogram (CV) measurements were carried out using an electrochemical workstation (CHI 631a, Shanghai Chenhua Co., China). Pt wire and a standard calomel electrode (SCE) were served as the counter and reference electrodes, respectively. All the potentials are presented with reference to the SCE. The glassy carbon electrode loaded with the as-prepared Au-Pd NCs was electrochemically cleaned by continuous potential cycling between  $-0.20$  and  $0.90 \text{ V}$  at  $50 \text{ mV}\cdot\text{s}^{-1}$  in  $0.5 \text{ mol/L H}_2\text{SO}_4$  until a stable CV curve was obtained. The electrochemical reactivity and electrochemically active surface area of the catalysts were determined by the area of the hydrogen desorption peaks in the CV measurement performed in  $0.5 \text{ mol/L H}_2\text{SO}_4$  electrolyte at a scan rate of  $50 \text{ mV}\cdot\text{s}^{-1}$  ( $25 \text{ }^\circ\text{C}$ ).

## Results and discussion

### Synthesis of Au-Pd bimetallic tripods enclosed by {411} high-energy facets with single-twinned structure

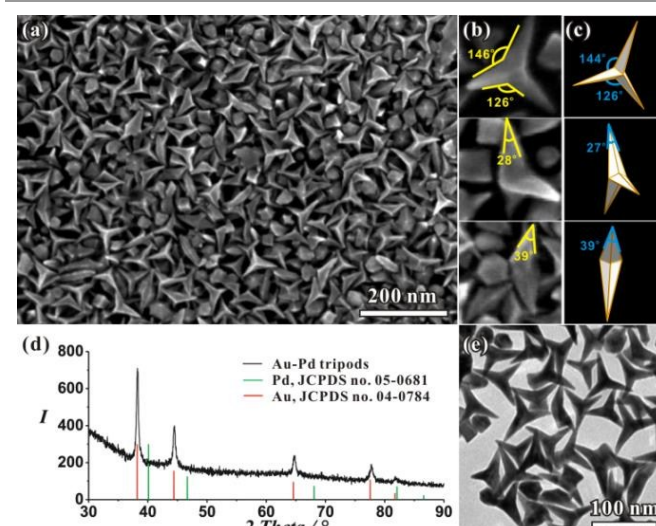


**Fig. 1** (a) Typical SEM image of the as-prepared Au-Pd tripods. (b, c) A series of high-magnification SEM images and corresponding model of the tripod NCs viewing from different orientations. (d) XRD pattern and (e) Typical TEM image of the as-prepared Au-Pd tripods.

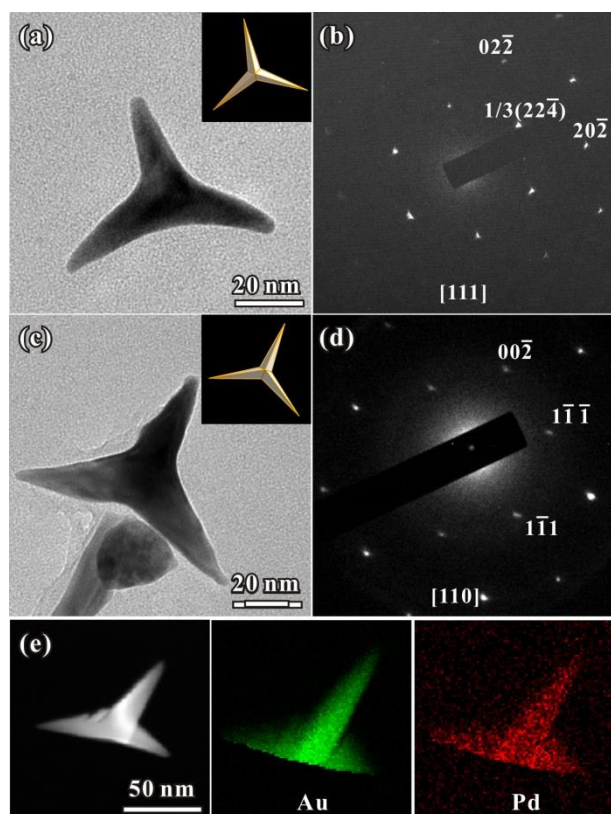


**Fig. 2** (a-d) TEM images and the corresponding SAED patterns of one individual Au-Pd tripod enclosed by the  $\{hkk\}$  facets oriented along the (a, b)  $[111]$  and (c,d)  $[\bar{3}\bar{2}\bar{3}]$  direction, respectively. (e) The typical STEM image and elemental scanning images of one Au-Pd tripod.

In our previous work, we obtained Au-Pd nanocubes with  $\{100\}$  surfaces exposed when using CTAC as the surfactant.<sup>38</sup> With the introduction of small amount of CTAB into the system, the products are evolved to tripods. Fig. 1a shows the typical SEM image of the product prepared via a facile wet-chemical reduction route by using  $\text{H}_2\text{PdCl}_4$  and  $\text{HAuCl}_4$  as metal sources and L-ascorbic acid as reductant in the presence of CTAC, CTAB and  $\text{Cu}(\text{CH}_3\text{COO})_2$ . As shown in Fig. 1a, the tripods were the main product with a high yield. The average length of the arms of the tripods was measured to be about 50 nm. The centre parts of the tripods are thicker than the top of the arms, indicating the formation of a concave right-bipyramid structure. By surveying from three different orientations (Fig. 1b), it can be observed that the as-prepared tripods contain a twin plane. The mirror symmetry of the tripods suggests that a  $(111)$  twin plane bisects its two single-crystal parts. Every single-crystal part of the special tripod can be thought to be evolved from a concave cube by cutting the model along  $\{111\}$  surface and then push the vertex of the tripod to the center (see Fig. S1 in the supporting information). Furthermore, these tripods in Fig. 1b can be matched well by a same tripod schematic model exposed by  $\{411\}$  high-energy surface projected from different orientation as shown in Fig. 1c. The structure and phase of the as-prepared NCs was determined by the X-ray powder diffraction (XRD) as shown in Fig. 1d. The as-prepared tripod NCs can be determined as the *fcc* structure

based on the XRD peaks. Every diffraction peak appears very close to the peak positions of pure *fcc*-structured Au due to the dominant amount of Au. The lattice parameter of the as-prepared tripod NCs was calculated to be  $4.070(1)$  Å. According to the Vegard's law,<sup>39</sup> the crystal cell parameter of an alloy is linearly related to its composition. Hence, the Pd content in Au-Pd alloy can be determined to be  $4.5 \pm 0.1$  %. ICP-AES measurement gives a mole fraction of 4.8% for Pd in the sample, which agrees well with the XRD calculation result. Fig. 1e shows the typical TEM image of the Au-Pd tripods. The surfaces of tripods are smooth and no obvious contrast change can be found, indicating that no phase separation occurred during the reaction. However, it should be pointed out that the amount of Pd precursor plays a delicate role in the formation of Au-Pd tripods in the present case. When the amount of introduced  $\text{H}_2\text{PdCl}_4$  (1 mM) increased to 1 mL, the surfaces of tripods became rough as shown in Fig. S2a, suggesting parts of Au and Pd nucleated separately. If the control experiment was carried out in the absence of  $\text{H}_2\text{PdCl}_4$ , the final products are irregular Au NCs (Fig. S2b), indicating that an appropriate amount of Pd precursor is necessary for the formation of as prepared Au-Pd tripods.

The structural features of the as-prepared Au-Pd tripods were further revealed by TEM images and the selected area electron diffraction (SAED) patterns. Fig. 2a-2d showed the TEM images of two tripods viewing from  $[111]$  and  $[110]$  directions and their corresponding SAED patterns, respectively. The schematic model matched the as-prepared tripod well along the two directions, further confirming the surfaces of the tripods are exposed by  $\{411\}$  facets. It should be pointed that  $1/3(422)$  diffraction point appeared in the SAED pattern viewed along the  $\langle 111 \rangle$  direction, which demonstrated the presence of the twin defect in the *fcc* metal nanostructures. From the TEM images and SAED patterns, we can conclude that each arm of the tripods was grown along the  $\langle 211 \rangle$  direction. The HR-TEM images of one individual tripod further confirmed the  $\langle 211 \rangle$  growth direction of the arms (Fig. S3, a and b). Fig. 2e showed the HAADF-STEM image of one Au-Pd tripod. Elemental mapping obtained by the HAADF-STEM-EDS reveal that the NCs are definitely Au-Pd alloy. While the compositional line-scanning profiles across the single nanocrystal (Fig. S3, c and d) showed a rather homogenous distribution of both gold and palladium in each nano-crystal. The intensity of the line-scanning profiles got stronger when the scanning point moving from branch to the centre of the tripod, which also indicated that the tripods were evolved from right-bipyramid seeds.<sup>36</sup>

#### Synthesis of Au-Pd bimetallic bipyramids enclosed by $\{hkk\}$ high-energy facets with multi-twinned structure

Interestingly, when we only use CTAB as the surfactant (in the absence of CTAC), bipyramid-shaped NCs were formed in a high yield, as shown in Fig. 3a. Based on the SEM images, the percentage of bipyramids in the as-obtained sample of such a synthesis was typically higher than 80%. The average diameter measured at the middle part is about 200 nm, and the average length of the bipyramids is about 2.0  $\mu\text{m}$ . Fig. 3b illustrates a

high-magnification SEM image of the Au-Pd bimetallic NCs, from which we can see that the surfaces of the bipyramids are smooth and highly faceted. The TEM image in Fig. 3c shows one individual bipyramid and corresponding schematic model exposed by  $\{hkk\}$  high-energy facets. By carefully analysing the structure of the bipyramid, the angle between the two salient of the bipyramid is  $19^\circ$ , which matched well with the schematic model (Fig. S4, a and b). By measuring the geometric parameters of the Au-Pd bipyramid, we can determine that the surfaces of bipyramids range from  $\{611\}$  to  $\{711\}$  facets (Fig. S4, c and d). Fig. 3d shows the HAADF-STEM image of one part of the bipyramid as marked in Fig. 3c. Elemental mapping (Fig. 3, e and f) obtained from the EDS analysis further confirms that the bipyramids are consisted of a Au-Pd alloy. In addition, the mole fraction of Pd was measured to be 5.1% by ICP-AES, which is very similar with that of Au-Pd tripods.

The XRD pattern determined the *fcc*-structure of Au-Pd bipyramids, which is the same as Au-Pd tripods (Fig. 4a). Every diffraction peak appears slightly biased toward higher angle compared to the peak positions of Au, indicating the formation of Au-Pd alloy. The structural features of the as-prepared Au-Pd bimetallic bipyramids were also revealed by the TEM image and corresponding SAED pattern. As shown in Fig. 4b and c, the SAED pattern contains two sets of diffraction points (Fig. 4c). In addition, the square and rectangular symmetrical diffractions correspond to  $[001]$  and  $[\bar{1}\bar{1}\bar{2}]$  zone axes, respectively. The HR-TEM image (Fig. 4d) recorded from the region marked in Fig. 4b indicated that as-prepared bipyramids have five-fold structures. The HR-TEM image with a higher resolution (Fig. 4e) clearly shows the five-fold twinned plane. The lattice spacing was measured to be 0.24 nm, which is corresponding to the  $\{111\}$  lattice spacing of Au-Pd alloy. The angle between two directions of crystal lattice was measured to be  $108^\circ$ , which further proved the formation of five-fold twinned structure. Based on the above SAED results and the HR-TEM image, it can be concluded that the obtained Au-Pd bipyramids are of a five-fold twinned structure. Furthermore, the Pd nanorods reported by Sun et al. have exactly the same twinning structure and equatorial cross-section as the Au-Pd bipyramids.<sup>40</sup> They also mentioned that this structure is enclosed by  $\{hkk\}$  facets. Therefore, the dominant surfaces of the as-prepared Au-Pd bipyramids NCs can be concluded as  $\{hkk\}$  facets.

#### The synergistic effect of CTAC/CTAB and mechanism for the shape-evolution of Au-Pd alloy NCs

As the introduction of CTAC and CTAB has an obvious influence on the morphology of Au-Pd alloy NCs, we carried out a set of experiments to demonstrate the roles of CTAC and CTAB in the synthesis. Fig. 5 shows the SEM images of the as-prepared Au-Pd NCs with different morphologies with the CTAB/CTAC molar ratio increased step by step. Specifically, Au-Pd nanocubes with an edge length of 30 nm were obtained in the absence of CTAB (Fig. 5a).<sup>38</sup> The nanocubes have a single-crystal structure and are enclosed by  $\{100\}$  low-energy facets. With the molar ratio of CTAB/CTAC increased to 0.1:2.9, the

products are the mixture of nanocubes and tripods as shown in Fig. 5b. When the ratio of CTAB was increased to a CTAB/CTAC molar ratio of 0.3:2.7, we obtained uniform tripods with arms of 50 nm in length (Fig. 5c). When we further increased the amount of CTAB to reach a CTAB/CTAC molar ratio of 1:2, the tripods showed some change in terms of uniformity (Fig. 5d). If the molar ratio of CTAB/CTAC changed to 2:1, some bipyramids were formed together with tripods, as shown in Fig. 5e. When we only use CTAB as the surfactant in the absence of CTAC, bipyramids were also formed in a high yield (Fig. 5f).

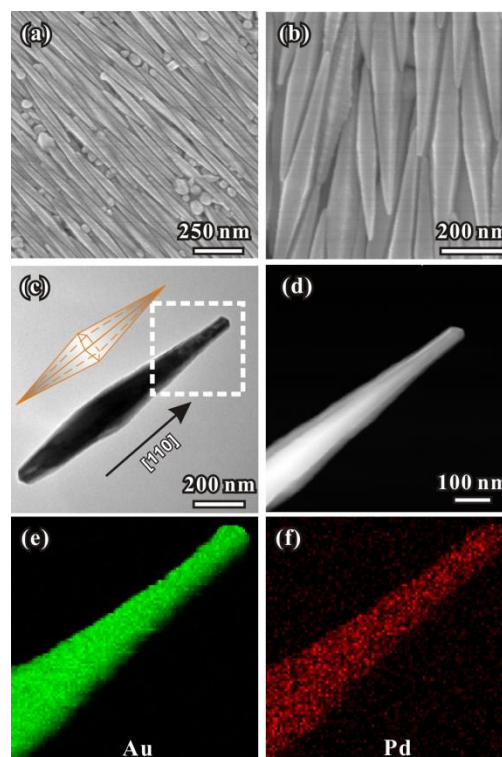


Fig. 3 (a, b) SEM images of the as-prepared Au-Pd bimetallic bipyramids. (c) TEM image of one individual Au-Pd bipyramid and the schematic model. (d) The typical STEM image and (e, f) elemental scanning images of one Au-Pd tripod from the regions marked in (c).

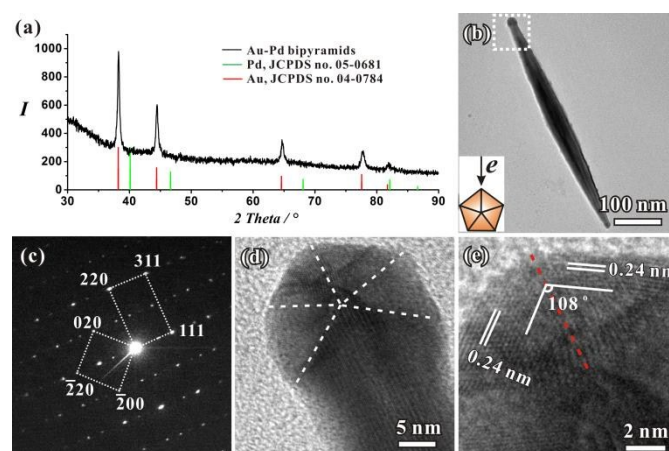
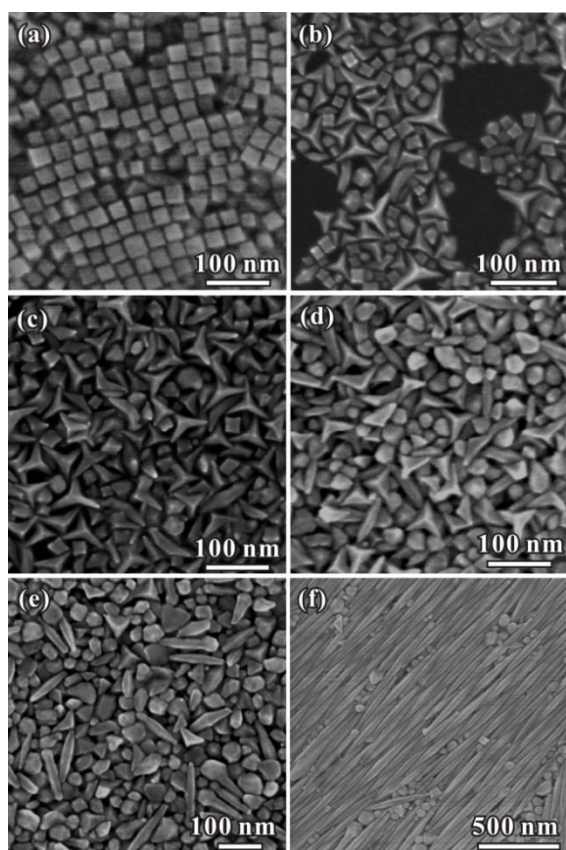


Fig. 4 (a) XRD pattern of the Au-Pd bipyramids. (b, c) TEM image and corresponding SAED pattern of one individual Au-Pd bimetallic bipyramid. (d, e) HR-TEM images of the Au-Pd bipyramid showing the formation of five-fold twinned structure.



**Fig. 5** SEM images of Au-Pd nanocrystals with different morphologies that were prepared using the standard procedure, with the introduction of different molar ratio of CTAB and CTAC: (a) 0: 3, (b) 0.1:2.9, (c) 0.3:2.7, (d) 1:2, (e) 2:1, and (f) 3: 0, whereas the total volume of the 0.04 M CTAC and CTAB was fixed at 3 mL.

On the basis of above results, we believe that the introduction of  $\text{Br}^-$  played a key role for the formation of the two novel structures. Owing to a larger stability constant for the coordination complex between  $\text{Pd}^{2+}$  ions with  $\text{Br}^-$  as compared to  $\text{Cl}^-$ , the introduction of CTAB into the solution should result in the formation of  $\text{PdBr}_4^{2-}$  complex ions via ligand exchange. The slow reduction kinetics induced by the coordination between  $\text{Br}^-$  and  $\text{Pd}^{2+}$  ions caused a relatively low deposition rate of Pd onto the NCs. Besides, Pd usually localizes on the higher-energy features of the nanocrystals during the co-reduction.<sup>30,36,41</sup> The growth rate of atoms on high-index surfaces became slower, which caused the NCs were exposed by relative high energy surfaces. On the other hand, the products should tune their structures to minimize the total Gibbs free energies during the crystal growth process. With the formation of right-bipyramid seeds containing a twin plane and fivefold twinned seeds, the surface-to-volume ratios was decreased, resulting in a smaller surface area.<sup>42,43</sup> As a result, the single crystal seeds evolved to right-bipyramid seeds, and then to fivefold twinned seeds, with the increasing amount of CTAB. With the reaction proceeding, the right-bipyramid seeds and fivefold twinned seeds grew to tripods and bipyramids, respectively.

In our previous work, we found that the introduced  $\text{Cu}^{2+}$  played a key role for the formation of Au-Pd alloy. Herein, we

also carried out a set control experiments based on the standard procedure for the preparation of Au-Pd tripods, to examine the influence of  $\text{Cu}^{2+}$ . When no  $\text{Cu}(\text{CH}_3\text{COO})_2$  was increased in the system, a phase separation phenomenon was clearly observed by the TEM image (Fig. S5a). If the amount of  $\text{Cu}(\text{CH}_3\text{COO})_2$  (1mM) was increased to 2 mL, the as-obtained product mainly consisted of spherical shape Au-Pd NCs of 20~30 nm (Fig. S5b). ICP-AES result showed that Pd content is 4.9% in the alloy. These result indicated that, although  $\text{Cu}^{2+}$  is essential for the formation of Au-Pd alloy, a proper introduced amount is also critically important for the formation of tripods.

#### Electrocatalytic Activity of the Tripods and bipyramids toward Formic Acid Oxidation

As the Au-Pd bimetallic tripods and bipyramids contain twinned defects, together with exposed high-index surfaces, they are expected to exhibit high chemical activity. We used electrocatalytic oxidation of formic acid to investigate the catalytic properties of the Au-Pd alloy exposed by high-energy surfaces. For comparison, the cubic Au-Pd alloy obtained with the introduction of only CTAC (see Fig. 5a), as reference material, was measured under the same conditions. Fig. 6a shows cyclic voltammogram (CV) curves in a mixture of 0.50 M  $\text{H}_2\text{SO}_4$  + 0.25 M HCOOH solution, using the obtained Au-Pd tripods, bipyramids and cubes as working electrodes, respectively. The current densities were normalized to the electrochemically active surface areas (ECSAs), which were determined by the area of the hydrogen desorption peaks in the cyclic voltammetry measurement performed in 0.50 M  $\text{H}_2\text{SO}_4$  electrolyte at a scan rate of  $50 \text{ mV s}^{-1}$  (25 °C). Notably, the potential peaks for the Au-Pd tripods and bipyramids were positioned at 0.65 and 0.63 V with peak current densities of 4.65 and  $3.47 \text{ mA cm}^{-2}$ , respectively. Both of the Au-Pd alloy with twinned structures and high-energy facets exhibited better activities than the cubic Au-Pd alloy. To evaluate the electrocatalytic stability of the as-prepared Au-Pd alloy catalysts, chronoamperometric experiments were carried out (Fig. 6b). In this test, we found that the stabilities of Au-Pd tripods and bipyramids catalysts were all much better than that of Au-Pd cubes.

The enhanced activities of Au-Pd alloy were caused by the cooperation of high-index facets and the twinned structures. It has been widely studied that the properties of catalysts are highly dependent on their surface structures. The distinct performances of various types of surfaces were caused by the different coordination numbers of atoms on surfaces. As an example, the coordination number of atoms on {111}, {100} and {110} surfaces are 9, 8 and 7, respectively.<sup>44</sup> The corresponding surface energy was in the order of {111}<{100}<{110}, which is the reason why {110} usually exhibited better than the other two basic facets. For the high-index facets, the exposed surfaces contain more atom steps, resulting in high densities of low coordinated atoms. Hence, high-index facets can exhibit much better activities relative to low-index facets. With the formation of twinned structure, the disordered region at the boundary could cause a relative high free energy of the NCs.<sup>45,46</sup> In addition, the exposed surfaces of

boundaries between two parts of twinned structures are {211} facets.<sup>47</sup> The {211} facet have been proved as an active surface for accelerating the formic acid oxidation.<sup>48</sup> Therefore, it can be concluded that, both the high-index facets and twinned structures provided more active atoms for enhancing the activity of Au-Pd catalysts.

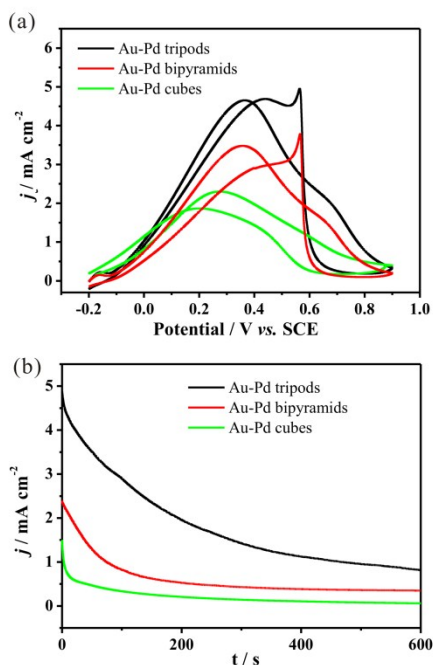


**Fig. 6** (a) CV curves measured on the Au-Pd tripods, bipyramids and spheres in an  $\text{N}_2$ -purged 0.50 M  $\text{H}_2\text{SO}_4$  + 0.25 M  $\text{HCOOH}$  solution, respectively. Scan rate: 50 mV/s. (b) current-time curves of formic acid oxidation measured on the three kinds of nanocatalysts in 0.50 M  $\text{H}_2\text{SO}_4$  + 0.25 M  $\text{HCOOH}$  solution at 0.30 V.

## Conclusions

In summary, two types of Au-Pd alloy NCs, tripods and bipyramids with twinned structures, are successfully synthesized by the synergistic effect of CTAC and CTAB. We proposed that with the different introduced ratio of CTAC and CTAB, the initial seeds formed during the nucleus process were tuned from single crystals to single-twinned seeds and fivefold-twinned seeds. During the overgrowth process, these three types of seeds evolved to the final products consisted of cubes, tripods or bipyramids, respectively. In addition, we also proved that  $\text{Cu}^{2+}$  played a key role for the formation of alloy structure. Due to the twinned structure and high-energy surfaces, the as-prepared Au-Pd tripods and bipyramids performed better activity for electrocatalytic oxidation of formic acid compared to the Au-Pd cubes.

## Acknowledgements

This work was supported by the National Natural Science Foundation of China (Grant Nos. 21171142, 21171141, 21131005, and 21333008), the National Basic Research

Program of China (Grant Nos. 2011CBA00508 and 2015CB932301).

## References

- 1 F. Kim, J. H. Song and P. Yang, *J. Am. Chem. Soc.*, 2002, **124**, 14316.
- 2 K. M. Bratille, H. Lee, K. Komvopoulos, P. Yang and G. A. Somorjai, *J. Am. Chem. Soc.*, 2007, **7**, 3097.
- 3 W. Niu, L. Zhang and G. Xu, *Nanoscale*, 2013, **5**, 3172.
- 4 P. Christopher and S. Linic, *J. Am. Chem. Soc.*, 2008, **130**, 11264.
- 5 Z. Jiang, Q. Kuang, Z. Xie and L. Zheng, *Adv. Funct. Mater.*, 2010, **20**, 3634.
- 6 W. X. Niu and G. B. Xu, *Nano Today*, 2011, **6**, 265.
- 7 K. Zhou and Y. Li, *Angew. Chem. Int. Ed.*, 2012, **51**, 602.
- 8 Y. Sun, *Nanoscale*, 2010, **2**, 1626.
- 9 Q. Kuang, X. Wang, Z. Jiang, Z. Xie and L. Zheng, *Acc. Chem. Res.*, 2014, **47**, 308.
- 10 B. Lim, M. Jiang, P. H. C. Camargo, E. C. Cho, J. Tao, X. Lu, Y. Zhu and Y. Xia, *Science*, 2009, **324**, 1302.
- 11 C. L. Lu, K. S. Prasad, H. L. Wu, J. A. A. Ho and M. H. Huang, *J. Am. Chem. Soc.*, 2010, **132**, 14546.
- 12 Y. Yu, Q. B. Zhang, B. Liu and J. Y. Lee, *J. Am. Chem. Soc.*, 2010, **132**, 18258.
- 13 F. Wang, C. H. Li, L. D. Sun, H. S. Wu, T. Ming, J. F. Wang, J. C. Yu and C. H. Yan, *J. Am. Chem. Soc.*, 2011, **133**, 1106.
- 14 L. Zhang, J. Zhang, Z. Jiang, S. Xie, M. Jin, X. G. Han, Q. Kuang, Z. Xie and L. Zheng, *J. Mater. Chem.*, 2011, **21**, 9620.
- 15 S. Maksimuk, S. C. Yang, Z. M. Peng and H. Yang, *J. Am. Chem. Soc.*, 2007, **129**, 8684.
- 16 V. R. Stamenkovic, B. Fowler, B. S. Mun, G. Wang, P. N. Ross, C. A. Lucas and N. M. Markovic, *Science*, 2007, **315**, 493.
- 17 L. Zhang, J. Zhang, Q. Kuang, S. Xie, Z. Jiang, Z. Xie and L. Zheng, *J. Am. Chem. Soc.*, 2011, **133**, 17114.
- 18 J. Xu, T. White, P. Li, C. He, J. Yu, W. Yuan and Y. Han, *J. Am. Chem. Soc.*, 2010, **132**, 10398.
- 19 Y. W. Lee, M. Kim, S. W. Kang and S. W. Han, *Angew. Chem.*, 2011, **123**, 3528.
- 20 N. Dimitratos, A. Villa, D. Wang, F. Porta, D. Su and L. Prati, *J. Catal.*, 2006, **244**, 113.
- 21 D. I. Enache, J. K. Edwards, P. Landon, B. Solsona-Espriu, A. F. Carley, A. A. Herzing, M. Watanabe, C. J. Kiely, D. W. Knight and G. J. Hutchings, *Science*, 2006, **311**, 362.
- 22 J. Zhang, C. Hou, H. Huang, L. Zhang, Z. Jiang, G. Chen, Y. Jia, Q. Kuang, Z. Xie and L. Zheng, *Small*, 2013, **9**, 538.
- 23 J. W. Hong, D. Kim, Y. W. Lee, M. Kim, S. W. Kang and S. W. Han, *Angew. Chem.* 2011, **123**, 9038;
- 24 C. J. DeSantis, A. C. Sue, M. M. Bower and S. E. Skrabalak, *ACS Nano*, 2012, **6**, 2617.
- 25 N. Tian, Z. Y. Zhou, S. G. Sun, Y. Ding and Z. L. Wang, *Science*, 2007, **316**, 732.
- 26 Y. Ma, Q. Kuang, Z. Jiang, Z. Xie, R. Huang and L. Zheng, *Angew. Chem. Int. Ed.*, 2008, **47**, 8901.
- 27 T. Ming, W. Feng, Q. Tang, F. Wang, L. D. Sun, J. F. Wang and C. H. Yan, *J. Am. Chem. Soc.*, 2009, **131**, 16350.
- 28 J. Zhang, M. R. Langille, M. L. Personick, K. Zhang, S. Y. Li and C. A. Mirkin, *J. Am. Chem. Soc.*, 2010, **132**, 14012.
- 29 Q. N. Jiang, Z. Y. Jiang, L. Zhang, H. X. Lin, N. Yang, H. Li, D. Y. Liu, Z. Xie and Z. Q. Tian, *Nano Res.*, 2011, **4**, 612.
- 30 J. Zhang, L. Zhang, S. Xie, Q. Kuang, X. G. Han, Z. Xie and L. Zheng, *Chem. Eur. J.* 2011, **17**, 9915.

- 31 B. Y. Xia, H. B. Wu, X. Wang and X. W. Lou, *Angew. Chem. Int. Ed.*, 2013, **125**, 12563.
- 32 L. Zhang and C. Zhang, *Nanoscale*, 2013, **5**, 6074.
- 33 M. Jin, H. Zhang, Z. Xie and Y. Xia, *Angew. Chem. Int. Ed.*, 2011, **50**, 7850.
- 34 X. Xia, J. Zeng, B. McDearmon, Y. Zheng, Q. Li, and Y. Xia, *Angew. Chem.*, 2011, **123**, 12750.
- 35 J. Wu, L. Qi, H. You, A. Gross, J. Li and H. Yang, *J. Am. Chem. Soc.*, 2012, **134**, 11880.
- 36 X. Xia, S.-I. Choi, J. A. Herron, N. Lu, J. Scaranto, H.-C. Peng, J. Wang, M. Mavrikakis, M. J. Kim and Y. Xia, *J. Am. Chem. Soc.*, 2013, **135**, 15706.
- 37 X. Wang, S.-I. Choi, L. T. Roling, M. Luo, C. Ma, L. Zhang, M. Chi, J. Liu, Z. Xie, J. A. Herron, M. Mavrikakis and Y. Xia, *Nat. Commun.*, 2015, **6**, 7594.
- 38 L. Zhang, Q. Chen, Z. Jiang, Z. Xie and L. Zheng, *CrystEngComm*, 2015, **17**, 5556.
- 39 A. R. Denton and N. W. Ashcroft, *Phys. Rev. A*, 1991, **43**, 3161.
- 40 N. Tian, Z. Y. Zhou and S. G. Sun, *Chem. Commun.*, 2009, 1502.
- 41 C. J. DeSantis, A. A. Peverly, D. G. Peters and S. E. Skrabalak, *Nano Lett.*, 2011, **11**, 2164.
- 42 Z. Niu, Q. Peng, M. Gong, H. Rong and Y. Li, *Angew. Chem. Int. Ed.*, 2011, **50**, 6315.
- 43 S. Bao, J. Zhang, Z. Jiang, X. Zhou and Z. Xie, *J. Phys. Chem. Lett.*, 2013, **4**, 3440.
- 44 Y. Xia, Y. Xiong, B. Lim, and S. E. Skrabalak, *Angew. Chem. Int. Ed.*, 2009, **48**, 60.
- 45 C. Lofton and W. Sigmund, *Adv. Funct. Mater.*, 2005, **15**, 1197.
- 46 F. Baletto and R. Ferrando, *Phys. Rev. B*, 2001, **63**, 155408
- 47 X. Wang, M. Vara, M. Luo, H. Huang, A. Ruditskiy, J. Park, S. Bao, J. Liu, J. Howe, M. Chi, Z. Xie, and Y. Xia, *J. Am. Chem. Soc.*, 2015, **137**, 15036.
- 48 X. Xia, S.-I. Choi, J. A. Herron, N. Lu, J. Scaranto, H.-C. Peng, J. Wang, M. Mavrikakis, M. J. Kim and Y. Xia, *J. Am. Chem. Soc.*, 2013, **135**, 15706.